

## The Taiwanese-American Occultation Survey: The Multi-Telescope Robotic Observatory

M. J. LEHNER,<sup>1,2,3</sup> C.-Y. WEN,<sup>1</sup> J.-H. WANG,<sup>1,7</sup> S. L. MARSHALL,<sup>4,5</sup> M. E. SCHWAMB,<sup>6</sup> Z.-W. ZHANG,<sup>7</sup> F. B. BIANCO,<sup>2,3</sup> J. GIAMMARCO,<sup>8</sup> R. PORRATA,<sup>9</sup> C. ALCOCK,<sup>3</sup> T. AXELROD,<sup>10</sup> Y.-I. BYUN,<sup>11</sup> W. P. CHEN,<sup>7</sup> K. H. COOK,<sup>5</sup> R. DAVE,<sup>12</sup> S.-K. KING,<sup>1</sup> T. LEE,<sup>1</sup> H.-C. LIN,<sup>7</sup> S.-Y. WANG,<sup>1</sup> J. A. RICE,<sup>13</sup> AND I. DE PATER<sup>14</sup>

Received 2008 February 4; accepted 2009 January 22; published 2009 February 26

**ABSTRACT.** The Taiwanese-American Occultation Survey (TAOS) operates four fully automatic telescopes to search for occultations of stars by Kuiper Belt Objects. It is a versatile facility that is also useful for the study of initial optical GRB afterglows. This paper provides a detailed description of the TAOS multi-telescope system, control software, and high-speed imaging.

### 1. INTRODUCTION

The Taiwanese American Occultation Survey (TAOS) continuously monitors up to  $\sim$ 1000 stars with four telescopes at 5 Hz, for the purpose of detecting occultations of these stars by small ( $\gtrsim$ 1 km) objects in the Kuiper Belt and beyond. Installation of the first three telescopes and the first version of the control software was completed in 2005 January, and the survey was officially started shortly thereafter. Installation of the fourth telescope was completed in 2007 January, and four telescope operations commenced in 2008 August. The TAOS Collaboration has finished analysis of the first two years of three-telescope data, which comprise over 150,000 star-hours

of observations. The results of this analysis are presented in Zhang et al. (2008).

The principal science questions addressed with this survey are:

1. What are the number and size distribution of small ( $\sim$ 0.5–10 km in diameter) bodies in the trans-Neptunian region?
2. Is there an extension of the Kuiper Belt beyond 50 AU comprising bodies too small to have been detected in direct surveys?
3. What are the number and size distribution of objects (e.g., Sedna) in the extended disk of the Solar System?

The signatures we are searching for are brief reductions in flux from background stars due to occultations by small Kuiper Belt objects (KBOs) and Extended Disk objects (EDOs). The occultation survey technique is uniquely suited to the detection of such objects, since it is capable of detecting objects that are much fainter than the magnitude limit of any plausible direct survey (Bailey 1976). However, the occultation technique is difficult to implement in practice, so the project includes some important technology development goals. For more details on application of the occultation technique to searches for outer Solar System objects, see Bickerton et al. (2008), Nihei et al. (2007), Cooray (2003), Cooray & Farmer (2003), Roques et al. (2006), Chang et al. (2007), and Roques et al. (2003). For an overview of the TAOS Project, see Lehner et al. (2006), Chen et al. (2007), and Alcock et al. (2003). For more information on the Kuiper Belt, see Jewitt & Luu (1993), Luu & Jewitt (2002), Bernstein et al. (2004), and Trujillo et al. (2001). For more information on the extended disk, see Brown et al. (2004), Kenyon & Bromley (2004), Morbidelli & Levison (2004), and Brasser et al. (2007).

In addition to the primary science goals stated above, a rapid response capability was implemented on the TAOS system to observe optical counterparts to gamma-ray burst (GRB) events

<sup>1</sup> Institute of Astronomy and Astrophysics, Academia Sinica. P.O. Box 23-141, Taipei 106, Taiwan; mlehner@asiaa.sinica.edu.tw

<sup>2</sup> Department of Physics and Astronomy, University of Pennsylvania, Philadelphia, PA 19104.

<sup>3</sup> Harvard-Smithsonian Center for Astrophysics, Cambridge, MA 02138.

<sup>7</sup> Institute of Astronomy, National Central University, No. 300, Jhongda Rd, Jhongli City, Taoyuan County 320, Taiwan.

<sup>4</sup> Kavli Institute for Particle Astrophysics and Cosmology, Menlo Park, CA 94025.

<sup>5</sup> Institute for Geophysics and Planetary Physics, Lawrence Livermore National Laboratory, Livermore, CA 94550.

<sup>6</sup> Division of Geological and Planetary Sciences, California Institute of Technology, Pasadena, CA 91125.

<sup>8</sup> Department of Astronomy and Physics, Eastern University, Saint Davids, PA 19087.

<sup>9</sup> Department of Physics, University of California, Berkeley, CA 94270.

<sup>10</sup> Steward Observatory, Tucson, AZ 85721.

<sup>11</sup> Department of Astronomy, Yonsei University, 134 Shinchon, Seoul 120-749, Korea.

<sup>12</sup> Initiative in Innovative Computing, Harvard University, Cambridge, MA 02138.

<sup>13</sup> Department of Statistics, University of California, Berkeley, CA 94720.

<sup>14</sup> Department of Astronomy, University of California, Berkeley, CA 94720.

reported to the GRB Coordinates Network<sup>15</sup> (GCN). The TAOS system observed its first optical counterpart to a GRB in 2007 October (Wang et al. 2008). The follow-up capability is described in § 5.7.

### 1.1. Design Criteria

Implementation of an occultation survey for detection of small KBOs presents a number of challenges. First, such events have very short durations, typically about 200 ms (Nihei et al. 2007). Second, such events are extremely rare. Estimates of occultation event rates are model dependent, and range from as low as  $10^{-4}$  events per star per year (Bernstein et al. 2004) to as high as  $10^{-2}$  events per star per year (Pan & Sari 2005). (Note that when this survey was designed in 1996, occultation event rates as high as  $10^{-1}$  per star per year were predicted for objects down to 1 km in diameter, but the results of Bernstein et al. (2004) showed a likely break in the size spectrum at diameters of about 30 km, which lowered the expected event rate.)

The TAOS system was thus designed to meet the following criteria:

1. Make photometric measurements at a high sampling rate (5 Hz).
2. Continuously monitor enough stars ( $\sim 1,000$ ) to obtain a significant event rate.
3. Low ( $\lesssim 0.1 \text{ yr}^{-1}$ ) false-positive rate.

The rapid photometry is achieved by means of the innovative use of an otherwise conventional CCD camera (described in § 4). An adequate number of stars can be imaged by a modern CCD camera mounted on a small (50 cm), fast ( $f/1.9$ ) telescope with a wide field of view ( $3 \text{ deg}^2$ ).

Achieving the goal of a low false-positive rate was a primary driver of the design. Our goal was to be able to measure a rate of stellar occultations by KBOs of one event per 1000 stars per year of observing time. We make  $\sim 10^{10}$  photometric measurements per year, from which we want to derive less than one spurious occultation. The false-alarm probability per observation must therefore be exceedingly small if the results of the survey are to be interpreted with confidence. We control false alarms by requiring joint detections in an array of four independent robotic telescopes. False positives of terrestrial or atmospheric origin (such as birds, aircraft, extreme atmospheric scintillation events, etc.) are eliminated by this requirement. False positives due to main belt asteroids can be eliminated by automated followup of detected events at a nearby, larger telescope. However, this would require a real-time analysis pipeline, which has not yet been implemented for this project. The telescopes are spaced far enough apart that scintillation events are unlikely to affect all of the telescopes simultaneously. Note, however, that the telescopes are close enough that any

occultation events would be detected by all four telescopes (see Nihei et al. (2007) for a detailed description of occultation events from objects in the Outer Solar System). Finally, note that the redundancy in the multi-telescope system also greatly enhances the credibility of the reported results. It would be difficult to credibly report on rare occultation events that were seen in only a single telescope.

This paper will specifically address the first two of the design criteria listed. A detailed description of the survey system (both hardware and software) will be presented, and the implementation of the survey system to address the design criteria will be discussed. We have developed statistical analysis techniques which make efficient use of the multi-telescope data to limit the false-positive rate and provide a credible result, however, discussion of these techniques is outside the scope of this article. An introduction to the statistical analysis methods used by the TAOS project can be found in Liang et al. (2004), and a discussion of the application of these techniques will appear in a future article (M. J. Lehner et al. 2009, in preparation).

## 2. THE SITE

The telescopes are installed atop Lu-Lin Mountain (longitude  $120^\circ 50' 28''\text{E}$ ; latitude  $23^\circ 30'\text{N}$ , elevation 2850 m), in the Yu Shan (Jade Mountain) area of Taiwan. The median seeing is  $1.3''$ , with  $\sim 100$  clear nights per year. Most of the poor nights occur during the rainy season (May–September). Since the beginning of 2005, TAOS has averaged  $\sim 400$  hours per year of actual observing, an average of four hours per clear night. High humidity is typically the reason that the observing hours are limited on clear nights. (Plans are currently being developed to start a new survey at a drier site.)

The telescopes have separations ranging from 6 m to 60 m (see Fig. 1). These separations are sufficient to eliminate most, if

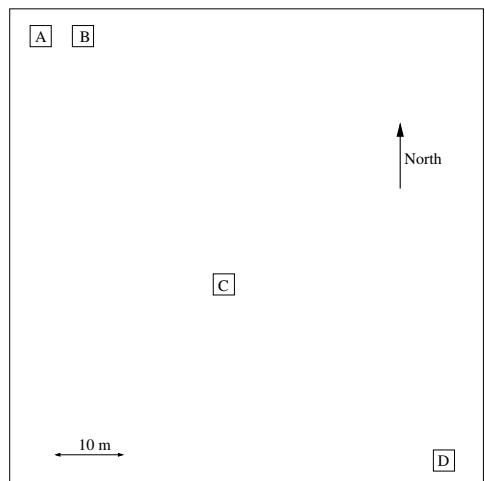


FIG. 1.—Layout of the four TAOS telescopes at Lu-Lin Observatory.

<sup>15</sup> See <http://gcn.gsfc.nasa.gov/>, see also Barthelmy et al. (1998)

not all, false positives arising from extreme scintillation events. Note that the original design for the TAOS project had the fourth telescope located 7 km to the west of the Lu-Lin site (King 2001). The reason for this design feature was that differences in the timing of an event would give a measurement of the relative velocity of the occulting object, thus allowing the object distance to be estimated. This plan was abandoned for several reasons. First, the development of the second site was logistically very difficult, and hence extremely expensive. Second, an occultation shadow crossing the Lu-Lin site would cross the second site only during part of the year, due to the obliquity of the Earth. Third, our 5 Hz sampling rate is not nearly fast enough to give a velocity measurement sufficiently accurate to provide a reasonable estimate of the distance. Finally, it was determined that a four-telescope system would provide significantly better statistical identification of false positives than a three-telescope system, as well as enable detection of smaller objects. These details will be described by M. J. Lehner et al. (2009, in preparation).

### 3. THE HARDWARE

#### 3.1. The Telescopes

The four identical telescopes were manufactured by Torus Technologies (now Optical Mechanics, Inc.). The TAOS telescopes were designed to be compact, and the optical design was based on the system requirement to cover a large number of stars using a camera with a single CCD chip. Based on the objectives of affordable cost and ease of manufacturing, a 50 cm aperture was chosen. Each telescope is a Cassegrain system with the focal plane located behind the primary mirror (see Fig. 2). In order to provide the fast-converging beam for a wide field of view, a parabolic primary mirror with f/1.5 is used. Combined with a f/3.6 spherical secondary mirror (25 cm diameter), the overall f ratio is about 1.9, with an effective field of view of 3 deg<sup>2</sup>. With a 14  $\mu\text{m}$ -pixel CCD, the plate scale is about 3'' pixel<sup>-1</sup>, which undersamples the seeing of the site. The effective collecting area is about 1875 cm<sup>2</sup>. The wide-field correctors consist of five lenses to provide a flat focal plane. Four different materials were used for the chromatic correction. The design criterion was to provide 60% of the enclosed energy within one pixel area within the passband between 500 and 750 nm. The design and modeling of the telescope was done using the ZEMAX™ software package<sup>16</sup>. The optical layout is shown in Figure 3 and the detailed parameters for the design are summarized in Table 1.

Each telescope is controlled by an Oregon Micro Systems PC68 card. The HA and Dec axes are driven by friction wheels which are powered by Bearing Engineers, Inc. Advanced Vector Servo systems. The axis positions are monitored by Renishaw

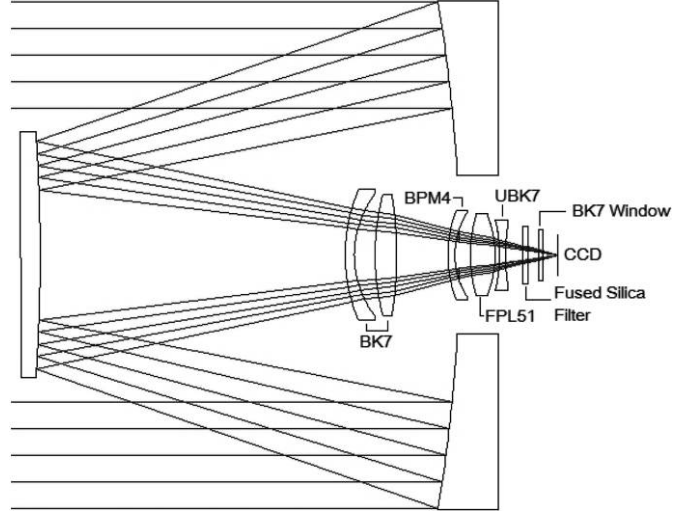


FIG. 2.—Optical layout of the TAOS telescopes.

RGH24 rotary encoders with 0.27'' step<sup>-1</sup> resolution. The secondary focus position is set by a screw drive powered by an Oriental Vexta PK245-03B motor controlled by an Intelligent Motion Systems IB462 bipolar stepping motor driver.

All of the telescopes were delivered with strong spherical aberrations over the whole field, as well as significant astigmatism in the corners of the images. The primary mirror on the fourth telescope was found to have very severe surface defects which distorted the point-spread function (PSF) beyond any reasonable shape and size. Each of the telescopes was also found to



FIG. 3.—TAOS B telescope.

<sup>16</sup> See <http://www.zemax.com/>

TABLE 1  
OPTICAL COMPONENTS OF THE TAOS TELESCOPES

| Element                | Radius of Curvature<br>(mm) | Axial Thickness<br>(mm) | Clear Aperture<br>(mm) | Conic Constant | Material |
|------------------------|-----------------------------|-------------------------|------------------------|----------------|----------|
| Primary mirror .....   | −1496.332                   |                         | 505.910                | −1             | Pyrex    |
|                        |                             | −418.142                |                        |                | Air      |
| Secondary mirror ..... | −1795.977                   |                         | 244.953                | 0              | Pyrex    |
|                        |                             | 304.360                 |                        |                | Air      |
| Lens 1 .....           | 165.470                     | 9.000                   | 130.467                | 0              | BK7      |
|                        | 98.600                      | 20.778                  | 121.809                | 0              | Air      |
| Lens 2 .....           | 239.650                     | 21.356                  | 121.570                | 0              | BK7      |
|                        | −408.100                    | 51.233                  | 119.782                | 0              | Air      |
| Lens 3 .....           | 124.500                     | 7.000                   | 89.810                 | 0              | BPM4     |
|                        | 77.790                      | 15.419                  | 83.550                 | 0              | Air      |
| Lens 4 .....           | 142.550                     | 24.535                  | 81.705                 | 0              | FPL51    |
|                        | −108.870                    | 4.522                   | 77.973                 | 0              | Air      |
| Lens 5 .....           | −149.580                    | 6.000                   | 69.911                 | 0              | UBK7     |
|                        | 198.530                     | 17.030                  | 64.277                 | 0              | Air      |
| Filter .....           | ∞                           | 5.000                   | 57.061                 | 0              | BK7      |
|                        | ∞                           | 10.775                  | 55.433                 | 0              | Air      |
| Camera window .....    | ∞                           | 4.000                   | 50.037                 | 0              | Silica   |
|                        | ∞                           | 15.329                  | 48.681                 | 0              | Vacuum   |
| CCD detector .....     | ∞                           |                         | 41.070                 | 0              |          |

have severe mechanical and defects. We found that the mirrors would move by large amounts (the primary mirrors would move 4–5 mm as the telescope would slew from horizon to horizon, while the specified tolerance was <50  $\mu\text{m}$ ). We also found the tracking accuracy limited by backlash in the drive system reduction gears and bad bearings in the friction wheel assemblies. The secondary focus systems were found to have poor resolution in positioning and significant backlash.

We have made significant improvements to the telescopes such that they are now of sufficient quality for the requirements of the survey. First, in order to keep the mirrors accurately positioned, the entire mirror support structures for both the primary and secondary mirrors were redesigned and refabricated by engineers at Lawrence Livermore National Laboratory. Second, the friction wheel assemblies were redesigned and refabricated by engineers at the Institute for Astronomy and Astrophysics at Academia Sinica in Taiwan, and the reduction gears were replaced with Bayside model PX-34-050-LB (50:1) devices. Third, the secondary focus drive systems were completely redesigned by engineers at Academia Sinica. A Renishaw RGH22 linear encoder with 0.5  $\mu\text{m}$  resolution was added to each telescope to enable the secondary focus positions to be accurately set to within 1.25  $\mu\text{m}$  (the limiting resolution from the stepper motor and threading of the drive shaft). The encoders are equipped with limit switches, to keep the secondary mirror from bottoming out against the support structure in one direction and completely unscrewing from the support structure in the other direction. The encoder system is also equipped with a magnetic

reference mark to reproduce the home position within one motor step, which is needed for the automatic focus control (see § 5.4.7). Finally, the primary mirror of the fourth telescope was repolished and resurfaced by the Space Optics Group at the Korea Research Institute of Standards and Science in Daejeon, South Korea, and it is now of quality comparable to the three other primaries.

Due to the poor optical quality of the optical components, the actual enclosed energy within one pixel averages about 30% rather than the design goal of 60%. The best PSFs now range from 1.6 pixels (4.6") in the center of the image to 2.5 pixels (7.3") in the corners. This lowered the limiting magnitude of the survey. We have partially compensated for the reduced optical quality by an upgrade to the CCD camera from a low quantum efficiency, front illuminated device to a camera with a back illuminated CCD (as will be described in the following section). The limiting magnitude of the survey is now roughly  $R = 13.5$ , rather than our target of  $R = 15$ . We have made a careful search for the densest fields along the ecliptic (see § 6), and we are typically able to monitor fields with 300–500 stars, which is within a factor of 2–3 of our design goal. We have designed a Hartmann-Shack device to routinely check on the optical performance of telescopes.

### 3.2. The Cameras

Each telescope is equipped with a thermoelectrically cooled Spectral Instruments Series 800 CCD camera employing a thinned, backside-illuminated e2v 2048  $\times$  2052 CCD42-40

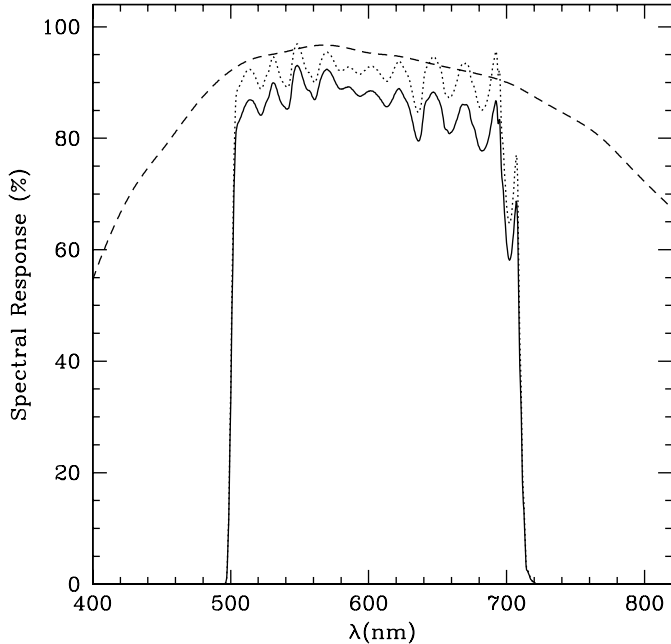


FIG. 4.—Spectral response of the camera system. Quantum efficiency of the CCD (dashed line), filter transmission (dotted line), total spectral response (solid line). Quantum efficiency data for the CCD was obtained from the e2v website at <http://www.e2v.com>.

chip.<sup>17</sup> The CCDs have  $13.5\text{ }\mu\text{m}$  pixels, corresponding to a plate scale of  $2.9''\text{pixel}^{-1}$ , and the total image area is  $27.6\text{ mm} \times 27.6\text{ mm}$ . There are two read channels, which work at a combined speed of  $1.8 \times 10^6\text{pixels s}^{-1}$ . The gain of each amplifier is set to about 2.0 ADU per electron, and the read noise is about  $10\text{ e}^-$ . The cameras are operated at a temperature of  $-20^\circ\text{C}$ , and the dark current is about  $0.05\text{ e}^- \text{sec}^{-1}\text{pixel}^{-1}$ . Each CCD chip has the e2v midband coating, providing peak quantum efficiency of over 93% and mean quantum efficiency over the planned spectral range of over 90%. Each camera has a custom-made filter (produced by Custom Scientific, Inc.) that provides over 80% transmission between  $500\text{ nm} \lesssim \lambda \lesssim 700\text{ nm}$ . The quantum efficiency of the CCD and filter transmission curves are shown in Figure 4.

The camera was delivered with a chiller for the thermoelectric cooler, but we found this device difficult to operate remotely. Since we do not need chilled water for our application, the chillers were replaced with ITW Cooling Systems 2500SS welding coolers, which are simply water circulators with fan-cooled radiators. Each cooler is equipped with a GEMS 2659 flow switch relay, designed to signal if the coolant flow stops for some reason.

<sup>17</sup>These chips are specified as  $2048 \times 2048$ , but there are four extra rows at the end of the CCD to act as a buffer for current leakage from the substrate. These rows must be read out in zipper mode, as they are shifted with every other row. However, the current leakage is negligible at our 5 Hz image cadence, so we can use these extra rows as actual imaging area.

### 3.3. Weather Monitoring

Accurate weather monitoring is an important component in any robotic telescope system, especially at a site prone to rain and high humidity. Most of the weather information is monitored by two Vaisala WXT510 weather stations. Each weather station is controlled and read through a serial port interface by a small Linux workstation. The two systems are used for redundancy, in case one of them fails. These weather stations provide information such as temperature, humidity, dew point, barometric pressure, and wind speed and direction.

To provide accurate measurement of the dew point under high humidity conditions, we installed a pair of Vaisala HMT337 humidity and temperature sensors. These devices are designed for high humidity applications, and specify an accuracy of  $\pm 1.7\%$  in relative humidity (or more importantly,  $\pm 0.3^\circ\text{C}$  accuracy in the dew point). These devices are run by the same computers that control the weather stations.

Each telescope enclosure is also equipped with a Vaisala DRD11A Rain Detector to detect precipitation at any level. The sensors output an analog voltage proportional to the amount of moisture on the sensor surface, and these voltages are monitored by a computer in each enclosure by a serial analog-to-digital converter. The devices are extremely sensitive, and will trigger closure of the enclosure lids immediately after the detection of a single droplet. Temperatures of the various parts of each optical assembly (primary mirror, secondary mirror, support struts, etc.) are monitored by Picotech Technology Ltd. thermocouple sensors.

The weather parameters of most concern are precipitation, humidity, wind, and temperature. We want the enclosure lids to close when there is any precipitation, and also when the humidity is high enough for condensation to form on the telescope components. Wind can damage the telescopes, and can even prevent lid closure (note that the lid effectively becomes a large sail during the opening and closing operations due to the clamshell design, as described in § 3.4). Wind is also a concern because of the effect on the tracking accuracy of the telescopes. As discussed in § 4, oscillations in the tracking accuracy due to wind will decrease the signal-to-noise ratio (S/N) achievable by the system. Temperature monitoring is necessary because many of the telescope components (e.g., the motor controllers) are not rated below certain temperatures. Temperatures of the optical and telescope assembly are compared to the dew point temperature so that we can close the enclosure lids if the telescopes get cold enough for condensation to form, and make real-time adjustments to our focus positions as the temperature changes (discussed in detail in § 5.4.7.).

To deal with these risks posed by weather, we defined a set of alarm thresholds for these various weather parameters. When one of these parameters crosses a threshold, a “WEATH\_BAD” alarm state is entered. In response to this alarm state, the lids of all of the enclosures will immediately be closed automatically. In addition, we have defined a second set of threshold levels that

TABLE 2  
WEATHER ALARM PARAMETERS

| Parameter   | Alarm On Threshold      | Alarm Off Threshold     |
|---|-------------------------|-------------------------|
| DRD11A voltage .....                                  | <2.5 V                  | >2.8 V                  |
| Relative humidity <sup>a</sup> .....                  | >95%                    | <94%                    |
| Dew point-temperature differential <sup>b</sup> ..... | <1.0°C                  | >1.5°C                  |
| Average wind speed .....                              | >20 km hr <sup>-1</sup> | <18 km hr <sup>-1</sup> |
| Maximum wind speed <sup>c</sup> .....                 | >30 km hr <sup>-1</sup> | <28 km hr <sup>-1</sup> |
| Minimum temperature .....                             | < -5.0°C                | > -3.0°C                |

(a) Value reported by HMT337 dew point sensor.

(b) Dew point value reported by HMT337 dew point sensor, temperature differentials calculated from HMT337 temperature reading and Picotech thermocouple measurements of telescope component temperatures.

(c) Measured over a 10-minute interval.

must be met for the WEATH\_BAD alarm state to be turned off. Once a WEATH\_BAD alarm state is entered, the weather parameters must remain past the second set of threshold values for 3 minutes before the alarm is turned off. This prevents the alarm from rapidly turning on and off when one of the parameters is hovering near the threshold. Threshold levels for each parameter are shown in Table 2.

### 3.4. The Enclosures

The TAOS enclosures (see Fig. 5) were designed to withstand the hurricane force winds accompanying the four or five typhoons that typically move through the region every summer. The enclosure walls consist of two 1 mm-thick steel plates separated by 5 cm of insulating foam, and are supported by 10 cm × 10 cm steel beams. The working area is about 3 m × 3 m. The lids are of a counterweighted clamshell-type design. They are constructed of polyurethane-filled fiberglass

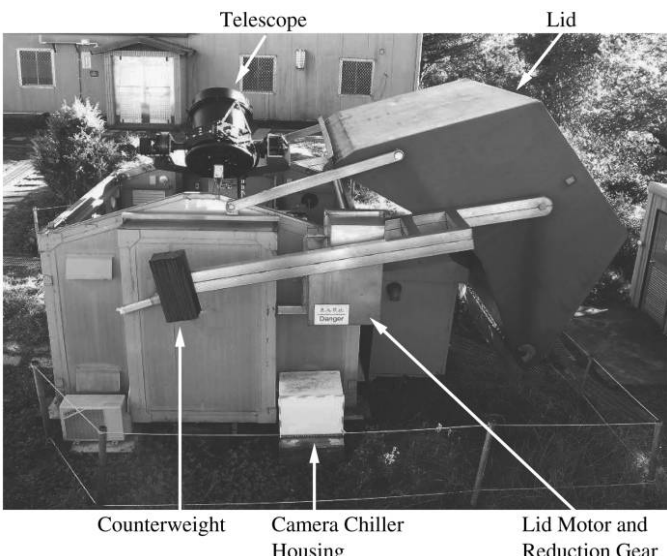


FIG. 5.—Enclosure for telescope TAOS A.

and were fabricated by the Aeronautical Research Laboratory of the Chungshan Institute of Science and Technology in Taiwan. Each lid is actuated by an ADLEE BM-370 brushless DC motor and a 1:400 worm reducer made by Shin Wei Ent Co. A custom control circuit is used to provide both manual operation and automated robotic operation through software. The time to open or close the lid is about one minute. In order to keep the lids operational during a power failure, each motor is powered by a SMR MCS1800 DC UPS made by Delta Electronics, Inc.

Each enclosure is equipped with air conditioning to keep the temperature of the telescope close to the anticipated night time temperature. This feature improves image quality by minimizing the temperature difference between the telescope components and the ambient temperature, and also minimizes the time used to find the best focus and focus change during the night.

Finally, each enclosure is equipped with a custom isolation transformer to protect the hardware from power surges induced by lightning, and all four TAOS enclosures are connected to the control building by 1 Gbps fiber optic cable for lightning protection, as well.

### 3.5. The Robotic Observatory Control System

In each TAOS enclosure, every subsystem other than the telescope and camera is controlled by a Sealevel Systems Model 8010 32 bit I/O card which is connected to a custom-built interface box. These boxes are based on a design used by the ROTSE Survey (Akerlof et al. 2003), but the design has been extensively modified. The boxes control the power to the cameras, the camera coolers, and the telescopes. The boxes also monitor the limit switches on the telescopes, and will automatically cut the power to a telescope if one of the switches is tripped. This power shutoff is done in hardware with a series of relay switches to ensure reliability. The chiller flow switches are also monitored by these hardware systems, and the software will turn off the thermoelectric cooler on the CCD and cut the power to the chiller should the flow unexpectedly stop.

The enclosure lids are also controlled by the interface boxes. The lids are opened and closed by asserting 12 V signal lines to the lid controller boxes. The limit switches to the lids are also monitored; once again, a set of relay switches will automatically cut the power to the open/close line when the open/close limit switch is tripped.

Finally, each box is equipped with an ICS Advent WDT5 watchdog module. This module must be pinged by the I/O card once every second, or it will close a set of relay switches which will automatically cut the power to the telescope and close the lid. If the computer crashes or one of the control daemons dies, the system will then be protected if any inclement weather arises before the system can be restarted.

#### 4. HIGH-SPEED PHOTOMETRY WITH ZIPPER MODE READOUT

The CCDs used for the TAOS project are described in § 3.2. The devices are  $2048 \times 2052$  e2v CCD42-40 chips. Each chip has two amplifiers, which allow for a combined readout rate of 1.8 MHz. It takes approximately 2.3 s to read out the entire frame, which makes our desired 5 Hz image cadence impossible without more than 90% dead time. To overcome this limitation, we designed a novel CCD readout method, which we call *zipper mode* (see Fig. 6).

As with conventional operation, when reading out in zipper mode, the telescope tracks the sky and stars are imaged onto the focal plane. However, instead of simply opening and closing the shutter for each exposure, the shutter is left open, and after 105 ms, a “row block” of 76 rows is read out. (The readout operation takes approximately 95 ms, so the readout time plus the exposure time is equal to our required sampling time of 200 ms.) This step is followed by another “hold” of 105 ms, then another row block is read out. This cycle may be repeated for extended periods of time, possibly up to several hours. Note that after 27 row blocks are read out ( $27 \text{ row blocks} \times 76 \text{ rows} = 2052 \text{ rows}$ , the total number of rows in the CCD), photoelectrons from every star on the focal plane will be read out in each subsequent row block. Every time 32 row blocks are read out,

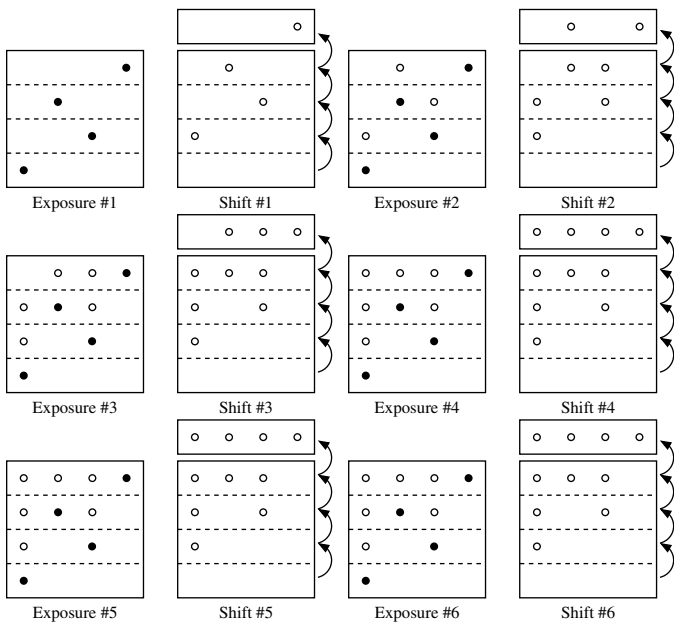


FIG. 6.—Illustration of zipper mode operation with the focal plane divided into four row blocks. Actual stars (*solid circles*), locations of electrons after shifts (*empty circles*). Note that after the fourth sequence of expose and shift operations, flux from all four stars is read out at each subsequent shift, although the flux from these stars was collected at different epochs.

the pixel data from all 32 row blocks are written to a single FITS<sup>18</sup> file.

The ability provided by zipper mode to read at 5 Hz comes with a cost in S/N, due to two properties inherent to zipper mode; any attempt to alleviate one of the problems exacerbates the other. First, photons from sky background are collected continuously during each hold and shift, while photons from a star are collected only during a single hold. Note that with row blocks of 76 rows, the pixels in a single row block contain photoelectrons collected from a total of  $2052/76 = 27$  holds. With a hold time of 105 ms and a sampling cadence of 5 Hz, the average recorded number of sky photoelectrons per pixel is thus a factor of  $27 \times 200/105 = 51.4$  times brighter than it would be after a simple, 105 ms exposure. Second, it takes just over 1 ms to read a single row. Photons from stars are still collected during this time, meaning that stars will leave streaks as a row block is read out, as can be seen in Figure 7. Faint stars are particularly vulnerable to this effect of flux contamination by streaks of bright stars. One could conceivably reduce the sky background by using row blocks with a larger number of rows, but this would reduce the effective exposure time relative to the readout time, and reduce the measured stellar brightness relative to the brightnesses of the streaks.

Ideally, the row block size would be an integral factor of 2052, the total number of rows on the CCD. (Stars near the edges of an image are missing a fraction of their flux, increasing uncertainty in the photometry, not only of the edge stars but also of their neighbors. This effect is minimized if the row block size is an integral factor of the number of rows in the CCD.) We found that the S/N was highest when the readout time was close to the exposure time; the integral factor of 2052 meeting this requirement is 76 rows.

Because of the increased sky background, zipper mode works well only for relatively bright stars. On a dark night, adequate S/N ( $\sim 7$ ) can be achieved with a star of  $V \sim 13.5$ , which consequently is the faintest magnitude we use in our occultation search.

This readout mode also requires accurate pointing and tracking throughout the duration of a zipper mode run, ideally to within a small fraction ( $\sim 0.1$ ) of a pixel. As shown in Figure 8, if there are significant oscillations in pointing error, then neighboring stars in a row block can move in different directions from their nominal positions over time. This movement can cause a significant reduction in S/N for closely neighboring stars in a row block due to varying blending fractions over time.

We did find both significant drifts and significant oscillations in the tracking of the telescopes, as shown in Figure 9. Reducing the magnitudes of these errors required significant hardware improvements (see § 3.1) and software modifications (see § 5.5). These modifications were completed in September of

<sup>18</sup> Flexible Image Transport System. See <http://heasarc.gsfc.nasa.gov/docs/heasarc/fits.html>.

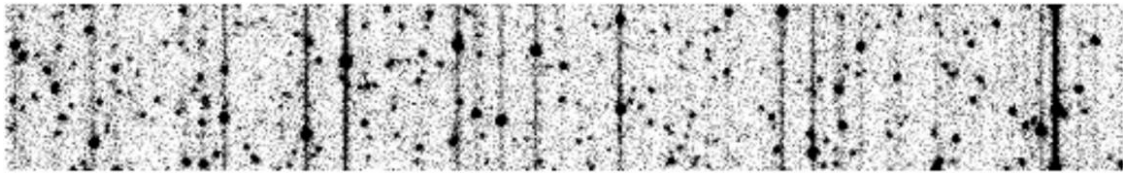


FIG. 7.—Example of a zipper mode image comprising a  $512 \times 76$  subsection of a  $2048 \times 76$  row block.

2005, so a large fraction of our first data set suffered from this problem. This issue will be discussed in Z.-W. Zhang et al. (2009, in preparation).

## 5. THE SOFTWARE

The control software for the TAOS system, like the observatory control boxes described in § 3.5, is adapted from the ROTSE Survey (Akerlof et al. 2003); however, it has been extensively modified for TAOS. Each component of the TAOS system is controlled by a separate daemon. A schematic of the daemons and their communication paths can be seen in Figure 10, and a description of each daemon is given in the following subsections.

Each enclosure has a dual-CPU Pentium 4 computer to control all of the hardware described in the previous section, and a

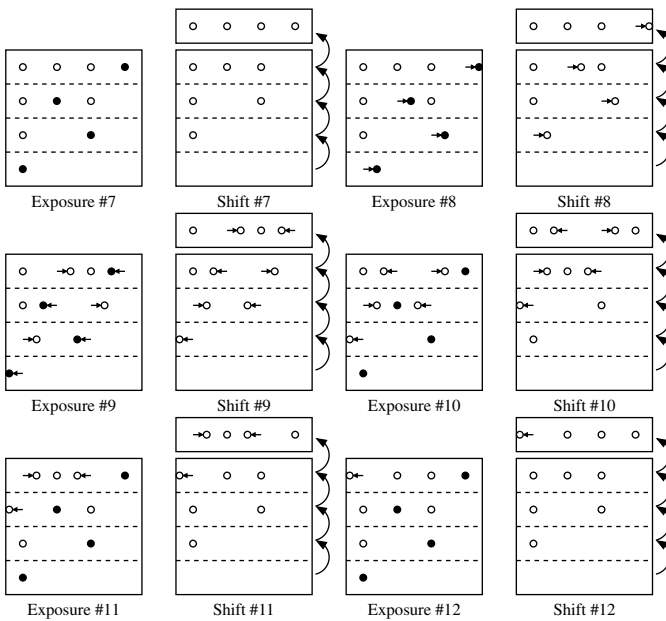


FIG. 8.—Continuation of zipper mode schematic in Fig. 6, illustrating effect of tracking errors throughout a zipper mode run. In this illustration, the telescope drifts to the left during exposure #8, moving the stars to the right of the image. During exposure #9, the telescope moves too far back to the right, moving the stars to the left of the image. Displacements of the stars from their nominal positions (*small horizontal arrows*). Note that the stellar flux that is read out in a row block is collected at different times, depending on where a star is located on the focal plane. Neighboring stars on a row block could therefore have offsets from their nominal positions in different directions.

small PC104 computer to control the telescope via an OMS PC68 Motion Controller Card. The main control computer is located in the TAOS control building, which also houses two small computers to monitor the two sets of weather stations (see § 3.3). All of the computers are running the Debian Sarge<sup>19</sup> distribution of Linux. Each of the main enclosure computers runs Linux kernel version 2.4.18 with the Kansas University Real-Time patch (KURT<sup>20</sup>) to provide microsecond timing resolution, which is important for synchronized zipper mode imaging at 5 Hz. The main control computer, weather station computers, and telescope control computers run Linux kernel version 2.6.8.

In order to provide accurate timing to the control computers (necessary for accurate telescope pointing and synchronized high-speed imaging), the clocks of all computers in the control system are synchronized via NTP<sup>21</sup> to the control computer. The NTP server on the control computer synchronizes to two NTP servers in Taiwan<sup>22</sup>.

### 5.1. Command and Status Message Passing

All command and status information is passed from computer to computer via standard INET sockets, using a custom message passing library. Command information is sent from the control computer directly to each enclosure computer.

Each computer has a Unix System V shared memory area which contains all status information from each enclosure, the control computer, and the weather computers. We call the shared memory area the “bulletin board.” Status information is kept up to date by the bulletin board daemon (*bbd*), which runs on each computer in the local network. Once every second, each instance of *bbd* updates every other instance with its local status information. Each daemon on the system thus has up-to-date information on every other daemon running on the system.

### 5.2. The Scheduler Daemon *braind*

The scheduler daemon *braind* controls the operation of the entire TAOS system. In particular, *braind* is responsible for initializing the system every night, scheduling zipper mode obser-

<sup>19</sup> See <http://www.debian.org>

<sup>20</sup> See <http://www.ittc.ku.edu/kurt/>

<sup>21</sup> Network Time Protocol. See <http://www.ntp.org/>.

<sup>22</sup> See <http://tick.stdtime.gov.tw>, <http://stdtime.sinica.edu.tw>

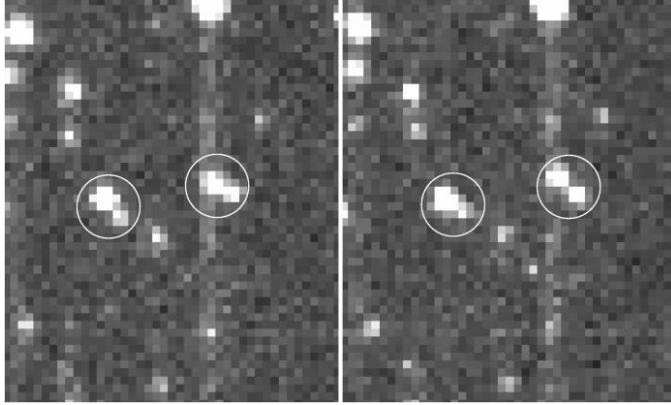


FIG. 9.—Two row block subsections taken at two different epochs. Note the two pairs of stars inside the circles. The two neighboring stars in the right circle are close together in the left image and have moved apart in the right (later) image. The two stars in the left circle moved closer together in the right image.

vations and GRB responses, keeping the telescopes focused, and shutting the system down at sunrise. The scheduler has four internal states, described in Table 3. While the Sun is above the horizon, the scheduler is in the SHUTDOWN state. In this state, the lid is closed and the telescope and camera are powered off. When the Sun goes below the horizon and the weather is good (see § 3.3), the scheduler will enter the GRBMODE state. In this state, the lid will be opened and the telescope and camera will be powered on. No zipper mode occultation survey data will be collected in this state; however, the system will respond to any GRB alerts that come in. (Zipper mode data are not very useful in twilight conditions, due to the increase in sky background; however GRB follow-up data could be useful under this circumstance.) When the Sun goes below an elevation of  $-18^\circ$  (i.e., the sky is sufficiently dark), *braind* enters STARTUP mode, and it will subsequently commence zipper mode observations for the occultation survey. If any GRB alerts come in during a zipper mode run, *braind* will interrupt the observations and schedule follow-up observations for the GRB event. At the end of the evening, when the Sun rises above  $-18^\circ$ , *braind* will go back into GRBMODE and will then only respond to GRB alerts. At sunrise, *braind* will go back into SHUTDOWN mode for the day, and will close the lids and power down the telescopes and cameras.

If *braind* is in the GRBMODE or STARTUP states when any of the weather parameter thresholds is reached, the system will go into STANDBY mode and close the lids. If the weather becomes good again, *braind* will go into either the GRBMODE or STARTUP state, depending on the elevation of the Sun. If the weather is bad when the Sun sets, the system will go straight into the STANDBY state from the SHUTDOWN state. Conversely, if the system is in the STANDBY state at the end of the night when the sun rises, it will go into the SHUTDOWN state.

Every day after sunrise and sunset, *braind* will schedule a set of dark images to be taken on each camera. At sunset, the dark

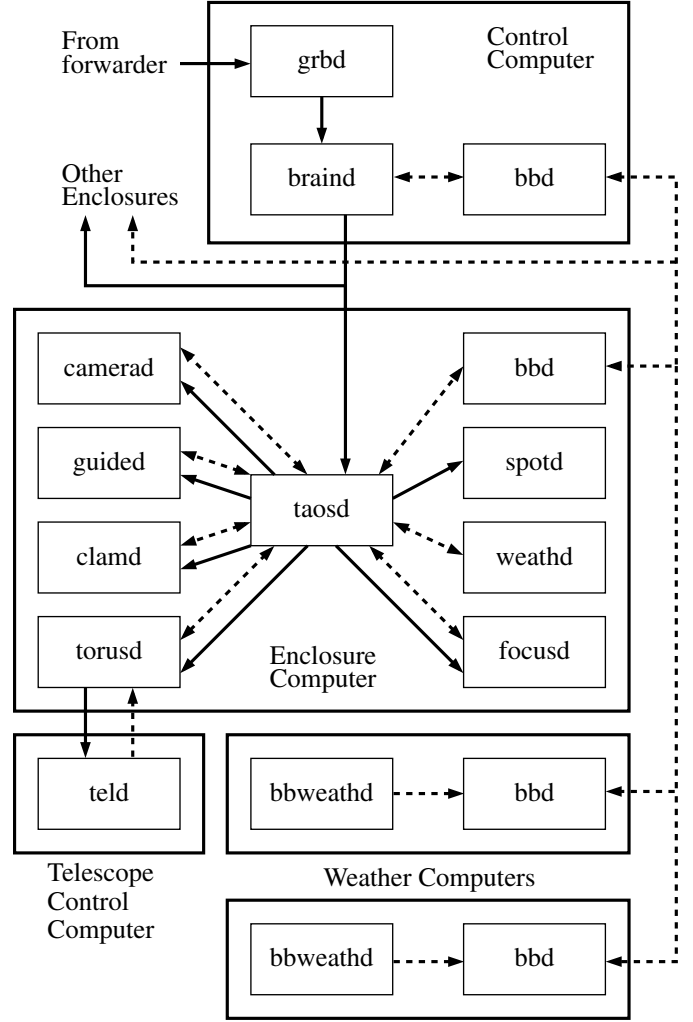


FIG. 10.—Schematic of the TAOS system control software. Control message bus (solid arrows), status message bus (dashed arrows). See text for details.

images are taken 300 s after *braind* enters the GRBMODE state, to give the camera ample time to cool down. At sunrise, the dark images are taken after the lids are closed but before the system enters the SHUTDOWN state. Each series of dark images comprises a set of 20 stare-mode dark images with 1 s exposures, and a series of 10 zipper mode dark images with the standard zipper mode parameters (5 Hz sampling, blocks of 76 rows, and 32 row blocks per FITS file).

### 5.3. The Weather Daemon *bbweathd*

The weather stations and dew point sensors described in § 3.3 are read by two instances of the *bbweathd* daemon, one instance for each set of one weather station and one dew point sensor. This daemon (as the name implies) reads both devices and publishes the information on the bulletin board for other software components to monitor. In addition, *bbweathd*

TABLE 3  
SCHEDULER STATES

| State          | Sun Elevation  | Weather Status | Lid Position | Telescope and Camera Power |
|----------------|----------------|----------------|--------------|----------------------------|
| SHUTDOWN ..... | $\geq 0^\circ$ | good or bad    | closed       | off                        |
| GRBMODE .....  | $< 0^\circ$    | good           | open         | on                         |
| STARTUP .....  | $< -18^\circ$  | good           | open         | on                         |
| STANDBY .....  | $< 0^\circ$    | bad            | closed       | on                         |

checks the measured weather parameters against a set of limits, and will set an alarm if adverse weather is detected. This alarm state is also written to the bulletin board for other daemons to monitor.

#### 5.4. Control Daemons

In addition to the instance of *bbd* described above, each enclosure computer runs a set of eight control daemons, each dedicated to a particular hardware component (or set of components) or high-level control task.

##### 5.4.1. The Master Control Daemon *taosd*

Every daemon running on the enclosure computer is a child of *taosd*. This daemon is responsible for forwarding commands from *braind* to the appropriate child daemon, and for monitoring the status of each of the children and passing the status information on to the local instance of *bbd*. Each child daemon has a dedicated Unix System \*V shared memory area which is used to pass command and status information to and from *taosd*. This daemon will automatically send commands to certain daemons based on the status information of other daemons (e.g., it will close the lid if adverse weather is detected).

##### 5.4.2. The Watchdog Daemon *sptd*

This simple daemon is responsible for pinging the watchdog module in the observatory control interface box described in § 3.5. It is designed to run independently of the rest of the daemons on the system to enable manual control (e.g., so the lid can be opened manually without the rest of the software running), however, when *taosd* is running, a simple “I'M ALIVE” command is expected from *taosd* at a rate of 1 Hz. If this command times out, *sptd* will die, the telescope will be stopped, and the lid will be closed. Thus if *taosd* crashes or otherwise is hung up for some reason, or if the enclosure computer itself crashes, the system will automatically go into a safe mode.

##### 5.4.3. The Local Weather Daemon *weathd*

While general weather information is monitored by *bbweathd*, a local weather daemon, *weathd*, runs on each enclosure computer as well. This daemon has three tasks. First, it monitors the Vaisala precipitation sensors described in § 3.3. Second, it monitors the local copy of the *bbweathd* information

on the bulletin board. If precipitation is detected or *bbweathd* reports adverse weather, a flag is set in the *weathd* shared memory segment, which will instruct *taosd* to abort current observations and close the lids. Finally, *weathd* monitors the telescope strut and mirror temperatures read by the thermocouple sensors attached to the telescope (see § 3.1), and compares these temperatures to the dew point reported by *bbweathd* to detect conditions requiring lid closure in order to prevent condensation on the telescope.

##### 5.4.4. The Telescope Command and Status Daemon *torusd*

The telescope is directly controlled by a small PC104 computer via an OMS PC68 motion controller card; communication between the main enclosure computer and the PC104 computer is handled by *torusd*. This daemon connects to the telescope control daemon *teld* (see § 5.5) over a set of four INET sockets: one for pointing and tracking control, one for the focus control, one for status information, and one for miscellaneous control commands.

##### 5.4.5. The Guide Daemon *guided*

While we have greatly improved the pointing and tracking capabilities of the system through both software and hardware modifications, we found the pointing was still inadequate for the survey. Accurate pointing (within 0.3") must be maintained throughout an entire zipper mode run, which can last as long as 2 h. As discussed in § 4, poor tracking can significantly decrease the S/N performance of the system, so it is desirable to keep the tracking as accurate as possible. While many surveys have a separate guiding imager, TAOS has the advantage that images are collected at a high rate, and we use this feature to enable our guiding system.

The *guided* daemon runs in two modes. During the initial pointing phase, we point the telescope to a field center and take a stare-mode image. This image is analyzed to find the actual RA and Dec of the image center, and a pointing offset is calculated, and a pointing adjustment command is sent to *torusd*; this process is repeated until the center of the image is within 0.1 pixel of the actual field center. In this way, at the beginning of a zipper run, all four telescopes are pointing to within 0.3" of the target field center.

The image analysis routine makes use of the standard software packages SExtractor (Bertin & Arnouts 1996) and *wcs tools* (Mink 2006), used in conjunction with the USNO-

B1.0 catalog (Monet et al. 2003). First, after an image is taken, the *wcstools* utility *imwcs* is run to find the World Coordinate System (WCS) keywords to transform RA and Dec to pixel coordinates. Second, SExtractor is run to find objects in the image. Third, the SExtractor output is used with the *wcstools* utility *immatch* to match the objects found by SExtractor. Finally, a set of polynomials (Malumuth & Bowers 1997) are fit to the data to convert from  $x$  and  $y$ , the pixel coordinates of each matched star calculated from the WCS coefficients, to  $x_p$  and  $y_p$ , the actual centroid locations reported by SExtractor. The polynomials are of the form

$$\begin{aligned}x_p &= C_0 + C_1x + C_2y + C_3x^2 + C_4xy + C_5y^2 + C_6x^3 \\&\quad + C_7x^2y + C_8xy^2 + C_9y^3 \\y_p &= D_0 + D_1x + D_2y + D_3x^2 + D_4xy + D_5y^2 + D_6x^3 \\&\quad + D_7x^2y + D_8xy^2 + D_9y^3,\end{aligned}\quad (1)$$

where  $C_i$  and  $D_i$  are the fit coefficients. After the fits are complete, these distortion coefficients and WCS keywords are used to calculate the RA and Dec of the center of the image, which is then used to calculate the pointing offset. The pointing offset is written to the *guided* shared memory status segment, which is then read by *taosd* and passed to *torusd* as a pointing adjustment command.

The second *guided* mode is the tracking mode. At the end of the initial pointing phase, 20 guide stars are selected from the stare-mode image. The stars are selected on criteria that include moderate brightness (i.e., bright enough to have good S/N characteristics but not so bright as to leave significant streaks in the zipper images), isolation (no close neighbors in zipper mode images), and distribution throughout the image so that the entire focal plane is well sampled. Note that a set of 32 consecutive row blocks is typically written to each FITS file, so there are effectively 640 guide stars in each image. Every 30 seconds, the last FITS image that was written to disk is analyzed. SExtractor is run on the image, and the centroids of the guide stars are found and compared with the original values. A pointing correction is calculated and written to the *guided* shared memory status segment, which in turn is read by *taosd* and passed as a pointing adjustment command to *torusd*. We find that the inherent tracking of the system is sufficient that the pointing drifts by much less than 0.1 pixel in the 30 s guiding update period, allowing *guided* to keep the pointing correct throughout an entire zipper mode run of up to two hours in duration.

The *guided* daemon also monitors image rotation throughout the course of a zipper run. Taiwan suffers from frequent earthquakes that can disrupt the polar alignment of the telescopes. We can thus learn in real time if the telescopes need realignment. Furthermore, *guided* reports the visibility conditions throughout the duration of a zipper mode run by monitoring the star count. Each time a zipper mode FITS file is analyzed for tracking adjustments, SExtractor reports the number of stars

to which it can fit a standard PSF. The star count is compared to the number of stars found at the beginning of the zipper mode run to indicate how the observing conditions vary throughout the run. In our fully automated observing mode, *taosd* will interrupt observations if the star count drops significantly. This usually occurs due to incoming clouds, or if the seeing degrades due to humidity or focusing problems. This real-time image quality analysis helps optimize our data collection, as we can interrupt a zipper mode run and refocus the telescope if necessary.

#### 5.4.6. The Lid Control Daemon *clamd*

The lid is opened and closed by a relatively simple daemon *clamd*. This daemon will assert an open or close signal to the lid controller on command, and monitor the open and close limit switches on the lid. The open and close signals are lowered when the appropriate limit switch is hit. The daemon will also set an alarm if the open or close operation times out, and this alarm will alert someone to fix the problem manually.

#### 5.4.7. The Focus Control Daemon *focussd*

The focus control daemon *focussd* has two tasks. The first is to analyze images taken during a focus sequence to determine the ideal focus position. A focus sequence consists of a series of 1 s exposures taken on a telescope with the secondary mirror at different focus positions. A total of 17 images are acquired while the focus position is moved by 15  $\mu\text{m}$  steps. A 1 K  $\times$  1 K subimage from the center of the focal plane is analyzed using SExtractor to find the average full width at half-maximum (FWHM) of each star in the image, and the focus position and medium FWHM are logged internally. After all of the images have been collected and analyzed, the FWHM data are fit to two straight lines, one line on each side of the point with the minimum FWHM. These fits are used to calculate the best focus position, which is then entered into a database along with the telescope component temperatures (reported by *weathtd*) and zenith angle of the telescope (reported by *torusd*).

The second function of the *focussd* daemon is to monitor the telescope component temperatures and zenith angle throughout a zipper mode run, and to look up the ideal focus position in the database. If the ideal focus position changes, the new position is written to the *focussd* shared memory status segment, where it is read by *taosd* and passed on to *torusd* as a focus adjustment command.

### 5.5. The Telescope Control Daemon *teld*

The system originally used the *telescopd* program from the OCAAS<sup>23</sup> software package to control the telescope. However,

---

<sup>23</sup> Observatory Control and Astronomical Analysis System, see <http://www.clearskyinstitute.com/>

we found three problems with this code that led us to the decision to write a completely new software package. First, the pointing model used by OCAAS did not accurately represent the pointing actually realized with the system. The residuals between the model and the true pointing were often as high as  $10''$ . Second, we found it difficult to generate the pointing model under OCAAS, where the pointing is adjusted by hand until a catalog star is centered on the image, a procedure that must be repeated for several stars. This very time-consuming process had to be done several times each year (after earthquakes), and for all four telescopes. It is also difficult to do remotely. Third, we found it difficult to implement a robust communication interface between *torusd* and the OCAAS software without a significant rewrite of the software.

The replacement daemon *teld* is a multi-threaded program, with separate threads dedicated to telescope pointing, focus control, status reporting, and a thread for master control (i.e., a parent thread to monitor the children). In addition, when a field is tracked, a new thread is spawned to control the telescope tracking directly. This thread runs with an elevated scheduling priority to keep the timing of the control loop accurate. Implementing a multi-threaded solution to the telescope control also required rewriting the driver for the PC68 motion controller card to make it thread safe. This was done by simply adding a semaphore to the driver which is raised whenever the card is accessed.

The daemon makes use of the SLALIB Positional Astronomy Library<sup>24</sup> to convert to and from J2000 RA and Dec to observed HA and Dec ( $h_{\text{obs}}$  and  $\delta_{\text{obs}}$ ). A custom pointing model derived from that used by the TPOINT software package<sup>25</sup> is used to convert  $h_{\text{obs}}$  and  $\delta_{\text{obs}}$  to actual encoder angles ( $\theta_h$  for the hour angle encoder and  $\theta_\delta$  for the declination encoder). The pointing model used is

$$\begin{aligned} h_1 &= h_{\text{obs}} - \text{TF} \cos \theta_{\text{lat}} \sin h_{\text{obs}} / \cos \delta_{\text{obs}} \\ \delta_1 &= \delta_{\text{obs}} - \text{TF} (\cos \theta_{\text{lat}} \cos h_{\text{obs}} \sin \delta_{\text{obs}} - \sin \theta_{\text{lat}} \cos \delta_{\text{obs}}) \\ &\quad - \text{KZ} \cos \delta_{\text{obs}} - \text{MZ} \sin \delta_{\text{obs}} - \text{FO} \cos h_{\text{obs}} \\ \theta_h &= -h_1 + \text{CH} \sec \delta_1 + \text{NP} \tan \delta_1 \\ &\quad + (\text{ME} \sin h_1 - \text{MA} \cos h_1) \tan \delta_1 + \text{IH} \\ \theta_\delta &= \delta_1 - \text{ME} \cos h_1 - \text{MA} \sin h_1 - \text{ID}, \end{aligned} \quad (2)$$

where  $h_1$  and  $\delta_1$  are temporary variables and  $\theta_{\text{lat}}$  is the geodetic latitude of the site; the 10 pointing model coefficients are described in Table 4.

After implementing *teld*, we found the typical residuals between the calculated and true positions to be less than  $10''$ . Using *teld* in conjunction with *guided*, we found that

TABLE 4  
POINTING MODEL COEFFICIENTS

| Coefficient     | Description   |
|-----------------|---|
| IH .....        | Hour angle home switch position                     |
| ID .....        | Declination angle home switch position              |
| CH .....        | Collimation error                                   |
| NP .....        | Nonperpendicularity of $h$ and $\delta$ axes        |
| MA .....        | Azimuthal polar alignment error                     |
| ME .....        | Elevation polar alignment error                     |
| TF .....        | Tube flexure  |
| FO .....        | Fork flexure  |
| KZ and MZ ..... | First order correction to declination encoder error |

we can track to well within  $0.3''$  for durations up to at least two hours.

We also implemented an automatic pointing model generation feature to the system. A set of 40 images is taken at a grid of locations on the sky, and the images are analyzed by *guided* to find the actual RA and Dec of the centers of the images. The subsequent arrays of RA, Dec,  $\theta_h$ ,  $\theta_\delta$ , and epoch are fit using the *amoeba* fitting routine, adapted from Press et al. (1994). This approach works much faster than the OCAAS method, especially when it must be done to all four telescopes several times each year. It also allows a new pointing model to be created remotely and automatically.

### 5.6. Collection of Zipper Mode Data

When the system is in STARTUP mode, *braind* will schedule a series of zipper mode runs. At the start of a run, *braind* will choose a standard TAOS field (see §6) based on criteria such as distance from the ecliptic plane, distance from zenith, and number of stars in the field. The scheduler will then instruct *torusd* to point all of the telescopes at the field center. Each telescope will then undergo a focus sequence (see § 5.4.7) and set the secondary focus to the best position. Once this is completed, each telescope will undergo a pointing correction, as described in § 5.4.5. Once all of the telescopes are pointing correctly, a set of three 1 s stare-mode images are acquired for diagnostic purposes. Next, the zipper mode sequence is started. Each camera system is sent a start time by *braind*; when the start time is reached, the shutters are opened and zipper mode readout is commenced. This 5 Hz readout process continues for a total of 90 minutes (as long as the weather remains good and no GRB alerts are received). Throughout the duration of the run, *guided* will keep the telescope pointed correctly. At the end of the run, a second set of three diagnostic stare-mode images are acquired, also with 1 s exposures. Finally, a sequence of 1 s stare-mode images is acquired with pointing offsets of  $0.8^\circ$  on a  $3 \times 3$  grid centered on the center of the field. This provides an effective mosaic image of  $\sim 11 \text{ deg}^2$  centered on the field, which is also used for diagnostic purposes.

<sup>24</sup> See <http://star-www.rl.ac.uk/>

<sup>25</sup> See <http://www.tpssoft.demon.co.uk/>

Throughout a zipper mode run, *braind* monitors the results of each command and the status of each daemon. If an error occurs, *braind* will attempt to recover by restarting any halted software and, if necessary, reinitializing the zipper mode run. If *guided* reports bad observing conditions, the zipper run will be aborted. A new field may be selected at this time, based on the scheduling criteria discussed earlier. If a new field is selected, *braind* will instruct the telescopes to point to it. In either case, the system will then undergo a new focus sequence to refocus the telescopes. If the weather is cloudy, this step will fail due to the lack of stars in the images. If refocusing fails, the system will wait for 300 seconds and then reattempt the focus sequence. This step will be repeated until the weather clears. If the cloudy weather does not clear, a new field may be selected by *braind*.

Every morning, all of the FITS images from the previous night (typically about 40 GB per telescope on a clear night) are archived to a local RAID server in the main control building. Once every month or so, the data are copied to a set of hard drives that are physically brought to Academia Sinica. The data are copied to a local data server, and then transferred to the Taiwan National Center for High-Performance Computing<sup>26</sup> for backup to tape. Finally, the data are copied over the internet to a second RAID server located at National Central University. This procedure results in three copies of the data in separate locations for secure, redundant data storage. The data are subsequently analyzed using two computer clusters (at Academia Sinica and National Central University) with a custom photometry package that will be described by Z.-W. Zhang et al. (2009, in preparation).

## 5.7. The GRB Alert Response System

The TAOS GRB response system consists of two components, the *forwarder* and the GRB daemon *grbd*. The *forwarder* simply monitors a socket connected to the GCN, and passes the information on to *grbd*. The *forwarder* runs on a machine with a more reliable internet connection than that available at Lu-Lin Observatory, so that if a GRB alert is sent out by the GCN when the connection to Lu-Lin is temporarily down, it can still be received by the *forwarder*, which will keep trying to forward the packet to *grbd* until it succeeds. We currently run the *forwarder* on a computer at the Institute for Astronomy and Astrophysics at Academia Sinica in Taipei.

When *grbd* receives a GCN alert packet from the *forwarder*, it parses the message and determines whether the reported event can be followed up by the TAOS system. If the GRB event is observable, *grbd* calculates an observation schedule and passes the request on to *braind*, which will interrupt any zipper mode operations and schedule the GRB follow-up observations.

TAOS has the advantage of multiple telescopes operating at the same site, which makes it possible to use different exposure times for the same event. Our observing scheme is optimized to have at least one telescope looking for fine structure in the light curves of bright events with short exposures, and two telescopes taking longer exposures for sensitivity to fainter afterglows. In the future, we may schedule one telescope to observe in zipper mode at 5 Hz to look for very bright and rapidly varying transients. To date, 10 GRB alerts were responded to by the TAOS system, and two afterglows ( $R$  16.5 and 16.8) have been detected (Wang et al. 2008).

## 6. FIELD SELECTION

In order to meet the survey requirements discussed in § 1.1, we needed to find a set of fields with sufficient numbers of stars. This task was complicated by the problem of streaks in the images from the brighter stars that occur with zipper mode readout, as discussed previously. It was therefore desirable to minimize the numbers of bright stars in the fields. An initial set of 167 fields was found, with varying characteristics such as number of stars and ecliptic longitude and latitude. More detailed information on the TAOS fields can be found on the TAOS website<sup>27</sup>. Note that this initial set is much larger than is needed; a large set was generated for the first phase of the survey in order to evaluate the fields in terms of S/N as a function of parameters such as sky background, stellar density, etc.

The USNO B1.0 catalog was used to select the fields (Monet et al. 2003). Initially, lists of stars were generated in  $300 \times 300''$  tiles. These tiles covered all of the sky with declinations in the range of  $-22^\circ < \delta < 68^\circ$ , which corresponds to elevation angles higher than  $45^\circ$  at the Lu-Lin site. After generation of over 4.6 million tiles, these smaller sections of the sky were merged into larger  $1.7^\circ \times 1.7^\circ$  lists of stars. The center of each small tile (except for those near the declination limits) became the center of the larger field. This process ensured overlap, allowing for the ability to maneuver around the bright stars ( $R < 9$ ) in the sky. Over four million of the large fields were generated.

A subset of these fields was selected according to the following characteristics:

1. Maximum number of stars in the field with  $R < 15$ .
2. Minimum number of bright stars ( $R \leq 9$ ).
3. Maximum coverage of the ecliptic.
4. Some control fields away from the ecliptic.
5. No nebulae or other astronomical phenomena.

These criteria were used to narrow down the list of viable fields. The field list was refined using a sorting routine to select fields with varying star densities. The main objective was to

<sup>26</sup> See <http://www.nchc.org.tw/>

<sup>27</sup> See <http://taos.asiaa.sinica.edu.tw/taosfield/>

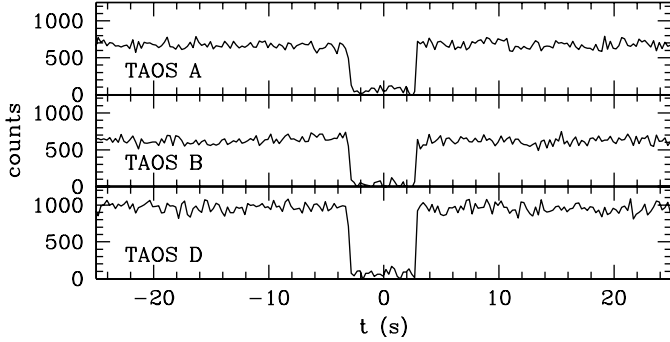


FIG. 11.—Light curves from three TAOS telescopes of the occultation of the star TYC 076200961 ( $V = 11.83$ ) by the asteroid Iclea ( $V = 14.0$ , diameter = 97 km) at UTC 12:35, 2006 February 6.

minimize the streaks in the zipper mode images while not significantly compromising on the total number of stars. Candidate fields that did not meet these criteria were cut from the list. Digital Sky Survey (DSS) images<sup>28</sup> were used to identify fields containing nebulae or other phenomena that made them unusable. The DSS images were also used to verify the accuracy of the USNO B1.0 catalog, particularly to ensure that there are no bright stars in the field that do not appear in the catalog.

Note that it was impossible to meet the stellar density requirement in all of the fields, as most of the fields along the ecliptic are very sparse (some of these fields have fewer than 100 stars). However, care was taken to find the densest fields available in these sparse regions, and it should be noted that the sparsest fields are visible mostly during the rainy summer months when observing is limited. Also note that high priority is given to observations of the densest fields in order to maximize the amount of useful data collected, and that the sparser fields are only observed when necessary due to the season and phase of the moon. The typical number of stars in the fields observed in our first data set was thus 300–500 stars (Zhang et al. 2008).

## 7. SYSTEM PERFORMANCE

To test the overall performance of the system, we have observed several predicted asteroid occultations<sup>29</sup>. Figure 11 shows the light curves of the occultation of the star TYC 076200961 ( $V = 11.83$ ) by the asteroid Iclea ( $V = 14.0$ , diameter = 31 km) at UTC 12:35, 2006 February 6. The event was observed by operating the three functioning telescopes at

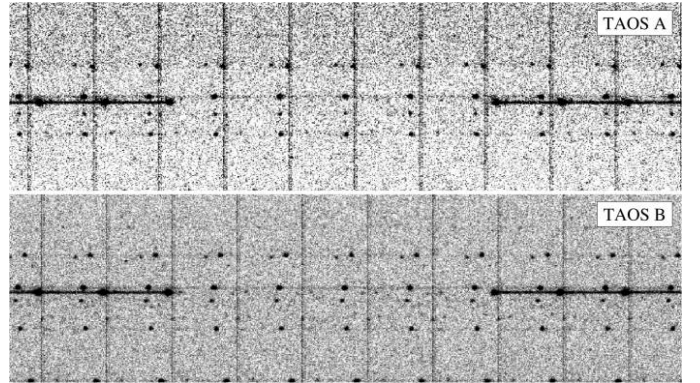


FIG. 12.—Zipper mode subimages from telescopes TAOS A and TAOS B of the occultation of the star HIP 050535 ( $V = 8.46$ ) by the asteroid Klemola ( $V = 15.7$ , diameter = 31 km) at UTC 12:10, 2004 June 5. Each subimage is an exposure of 0.25 s, with time increasing to the right. The vertical lines visible in each set of images are caused by a slight excess in dark current from the CCD substrate, and indicate the boundaries of the row blocks. These images were taken before the *guided* daemon was implemented, so the two telescopes have different pointing offsets and the occulted star is in a different location in the row block.

4 Hz. The event, which lasted for approximately 6 s, is clearly visible, indicating that the system is indeed capable of accurate, high-speed imaging. Figure 12 shows a series of zipper mode images of the occultation of the star HIP 050535 ( $V = 8.46$ ) by the asteroid Klemola ( $V = 15.7$ , diameter = 31 km) at UTC 12:10, 2004 June 5. This event had a short duration, lasting only 1.3 s.

These asteroid occultation events clearly illustrate that the TAOS system is capable of detecting short duration occultation events with multiple telescopes. The system has been collecting data for over three years with three telescopes, with the fourth telescope brought online in 2008 August. Since 2005 February, we estimate that TAOS has made over  $5 \times 10^{10}$  individual photometric measurements, and analysis of the first two years of data has been completed (Zhang et al. 2008).

This work was supported in part by the National Science Foundation under grant AST-0501681 and by NASA under grant NNG04G113G, both at the Harvard College Observatory. Work at Academia Sinica was supported in part by the thematic research program AS-88-TP-A02. The work at National Central University was supported by grant NSC 96-2112-M-008-024-MY3. SLM's work was performed under the auspices of the U.S. Department of Energy by Lawrence Livermore National Laboratory in part under Contract W-7405-Eng-48 and by Stanford Linear Accelerator Center under Contract DE-AC02-76SF00515. Work at Yonsei was supported by the KRCF grant to the Korea Astronomy and Space Science Institute. KHC's work was performed under the auspices of the U.S. Department of Energy by Lawrence Livermore National

<sup>28</sup> See <http://archive.stsci.edu/dss/>

<sup>29</sup> The asteroid occultation observations were based on the predictions of Dr. Isao Sato of the Nakano Star Gazers Club.

Laboratory in part under Contract W-7405-Eng-48 and in part under Contract DE-AC52-07NA27344. MJL wishes to thank Jeff Klein at the University of Pennsylvania for valuable advice

regarding the system hardware development. MES wishes to thank Jeff Goldader and Gary Bernstein at the University of Pennsylvania for advice on the TAOS field selection.

## REFERENCES

- Akerlof, C. W., et al. 2003, PASP, 115, 132  
 Alcock, C., et al. 2003, Earth Moon Planets, 92, 459  
 Bailey, M. E. 1976, Nature, 259, 290  
 Barthelmy, S. D. et al. 1998, in AIP Conf. Proc. 428, 4th Huntsville Symp. on Gamma-Ray Bursts, ed. C. A. Meegan, R. D. Preece, & T. M. Koshut (New York: AIP), 99  
 Bernstein, G. M., et al. 2004, AJ, 128, 1364  
 Bertin, E., & Arnouts, S. 1996, A&AS, 117, 393  
 Bickerton, S. J., Kavelaars, J. J., & Welch, D. L. 2008, AJ, 135, 1039  
 Brasser, R., Duncan, M. J., & Levison, H. F. 2007, Icarus, 191, 413  
 Brown, M. E., Trujillo, C., & Rabinowitz, D. 2004, ApJ, 617, 645  
 Chang, H.-K., et al. 2007, MNRAS, 378, 1287  
 Chen, W. P., et al. 2007, in IAU Symp. 236, Near Earth Objects, our Celestial Neighbors: Opportunity and Risk, ed. G. B. Valsecchi, & D. Vokrouhlický (New York: Cambridge Univ. Press) 65  
 Cooray, A. 2003, ApJ, 589, L97  
 Cooray, A., & Farmer, A. J. 2003, ApJ, 587, L125  
 Jewitt, D., & Luu, J. 1993, Nature, 362, 730  
 Kenyon, S. J., & Bromley, B. C. 2004, Nature, 432, 598  
 King, S.-K. 2001, in IAU Colloq. 183, Small Telescope Astronomy on Global Scales, ed. B. Paczynski, W.-P. Chen, & C. Lemme, ASP Conf. Ser. 246, 253  
 Lehner, M. J., et al. 2006, Astron. Nachr., 327, 814  
 Liang, C.-L., et al. 2004, Statist. Sci., 19, 265  
 Luu, J. X., & Jewitt, D. C. 2002, ARA&A, 40, 63  
 Malumuth, E. M., & Bowers, C. W. 1997, in The 1997 HST Calibration Workshop with a New Generation of Instruments, ed. S. Casertano, R. Jedrzejewski, T. Keyes, & M. Stevens, (Baltimore: Space Telescope Science Institute) 144  
 Mink, D. 2006, in ASP Conf. Ser. 351 Astronomical Data Analysis Software and Systems XV, ed. C. Gabriel, C. Arviset, D. Ponz, & S. Enrique, 204  
 Monet, D. G., et al. 2003, AJ, 125, 984  
 Morbidelli, A., & Levison, H. F. 2004, AJ, 128, 2564  
 Nihei, T. C., et al. 2007, AJ, 134, 1596  
 Pan, M., & Sari, R. 2005, Icarus, 173, 342  
 Press, W. H., et al. 1994, Numerical Recipes in C (New York: Cambridge University Press)  
 Roques, F., et al. 2003, ApJ, 594, L63  
 ———. 2006, AJ, 132, 819  
 Trujillo, C. A., et al. 2001, AJ, 122, 2740  
 Wang, J.-H., et al. 2008, ApJ, 679, L5  
 Zhang, Z.-W., et al. 2008, ApJ, 685, L157